

# Epigenomic and Transcriptomic Changes During Human RPE EMT in a Stem Cell Model of Epiretinal Membrane Pathogenesis and Prevention by Nicotinamide

Nathan C. Boles,<sup>1,7</sup> Marie Fernandes,<sup>2,7</sup> Tomasz Swigut,<sup>3</sup> Rajini Srinivasan,<sup>3</sup> Lauren Schiff,<sup>1</sup> Alvaro Rada-Iglesias,<sup>5</sup> Qingjie Wang,<sup>6</sup> Janmeet S. Saini,<sup>1</sup> Thomas Kiehl,<sup>2</sup> Jeffrey H. Stern,<sup>2</sup> Joanna Wysocka,<sup>3,4</sup> Timothy A. Blenkinsop,<sup>2,8,\*</sup> and Sally Temple<sup>1,8,\*</sup>

<sup>1</sup>Neural Stem Cell Institute, Rensselaer NY 12144, USA

<sup>2</sup>Icahn School of Medicine at Mount Sinai, New York, NY 10029, USA

<sup>3</sup>Department of Chemical and Systems Biology, Department of Developmental Biology, Stanford University, Stanford, CA 94305, USA

<sup>4</sup>Howard Hughes Medical Institute, Stanford, CA 94305, USA

<sup>5</sup>University of Cologne, Cologne 50931, Germany

<sup>6</sup>Stony Brook University School of Medicine, Stony Brook, NY 11794, USA

<sup>7</sup>Co-first author

<sup>8</sup>Senior author

\*Correspondence: [timothy.blenkinsop@mssm.edu](mailto:timothy.blenkinsop@mssm.edu) (T.A.B.), [sallytemple@neuralsci.org](mailto:sallytemple@neuralsci.org) (S.T.)

<https://doi.org/10.1016/j.stemcr.2020.03.009>

## SUMMARY

Epithelial to mesenchymal transition (EMT) is a biological process involved in tissue morphogenesis and disease that causes dramatic changes in cell morphology, migration, proliferation, and gene expression. The retinal pigment epithelium (RPE), which supports the neural retina, can undergo EMT, producing fibrous epiretinal membranes (ERMs) associated with vision-impairing clinical conditions, such as macular pucker and proliferative vitreoretinopathy (PVR). We found that co-treatment with TGF- $\beta$  and TNF- $\alpha$  (TNT) accelerates EMT in adult human RPE stem cell-derived RPE cell cultures. We captured the global epigenomic and transcriptional changes elicited by TNT treatment of RPE and identified putative active enhancers associated with actively transcribed genes, including a set of upregulated transcription factors that are candidate regulators. We found that the vitamin B derivative nicotinamide downregulates these key transcriptional changes, and inhibits and partially reverses RPE EMT, revealing potential therapeutic routes to benefit patients with ERM, macular pucker and PVR.

## INTRODUCTION

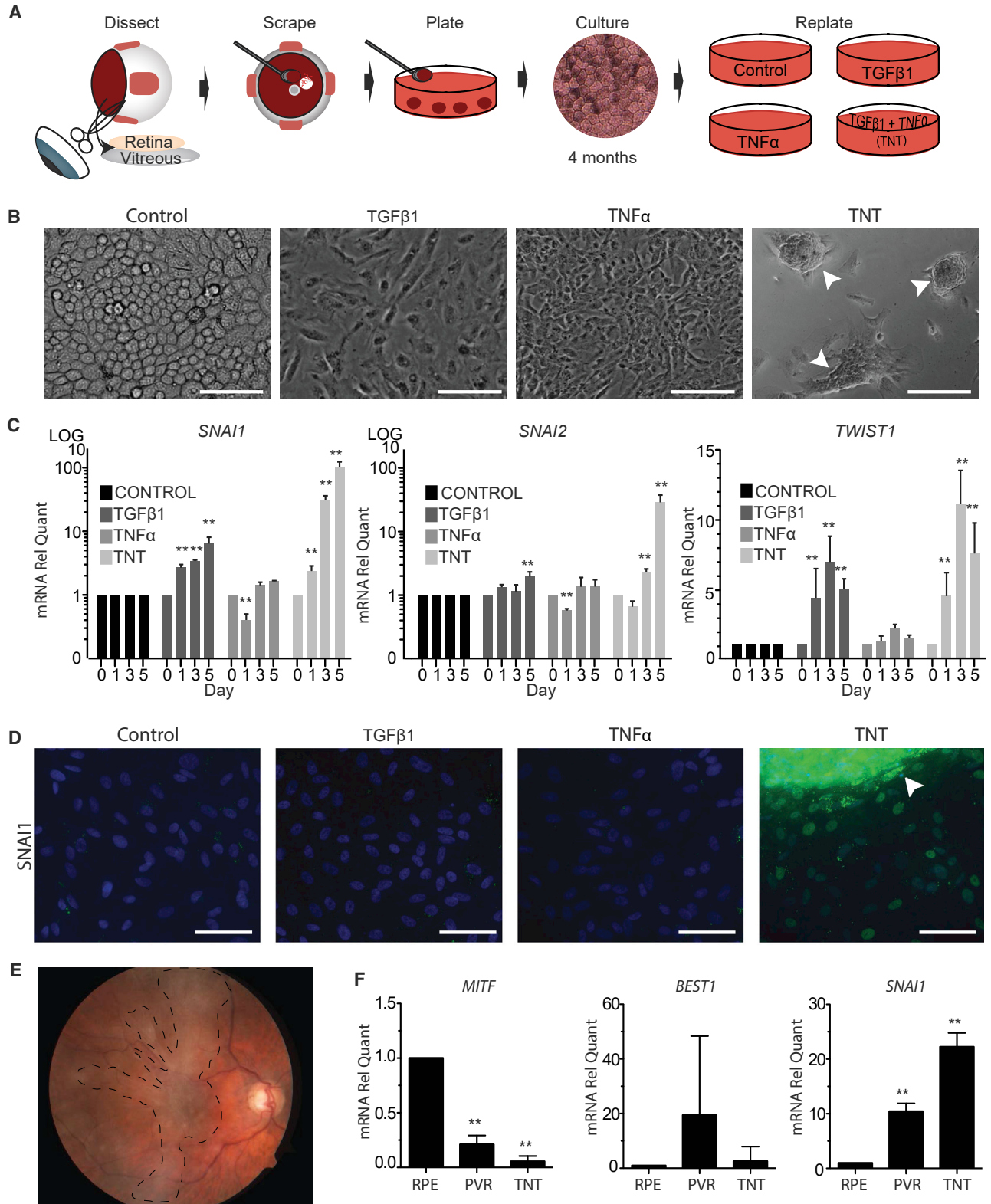
During epithelial to mesenchymal transition (EMT), epithelial cells change phenotype, lose cell polarity, and become migratory and proliferative. Pathological EMT can result in cell proliferation, invasion, and metaplasia (Kalluri and Weinberg, 2009). In the human retina, healthy retinal pigment epithelium (RPE) consists of a single, non-proliferative neuroepithelial cell layer that supports neural retinal function. RPE cells form a polarized monolayer with tight junctions, contributing to the blood-retina barrier. If triggered, RPE cells undergo EMT, delaminate from the epithelial layer, proliferate, and acquire mesenchymal characteristics. These mesenchymal-like RPE can contribute to epiretinal membrane (ERM) formation in macular pucker (Snead et al., 2008) or more aggressive proliferative vitreoretinopathy (PVR), characterized by contractile ERMs that can pull and damage the retina (Machemer, 1977; Tamiya and Kaplan, 2016). The molecular basis of pathological RPE EMT, including changes in gene expression and regulation, remain poorly understood.

Retinal tears due to vitreoretinal traction and retinal detachment are common preceding PVR (Girard et al., 1994; Machemer, 1988). RPE cells become dislodged from

their niche, are released into the vitreous through the retinal tears and become exposed to inflammatory cytokines that stimulate migration, proliferation, and PVR. Many of these cytokines, including transforming growth factor  $\beta$  (TGF- $\beta$ ) and tumor necrosis factor alpha (TNF- $\alpha$ ), are made by the RPE cells themselves or other cells in the pathological tissue, such as macrophages (Machemer, 1988; Nagasaki et al., 1998; Pastor et al., 2002). TGF- $\beta$  is increased in the vitreous of patients with PVR, correlated with PVR severity (Kita et al., 2008). TNF- $\alpha$  is also increased in the vitreous of patients with PVR and macular pucker (Korthagen et al., 2015). Studies of patient-derived PVR membranes reveal activation of both TGF- $\beta$  and TNF- $\alpha$  signaling pathways (Asato et al., 2013; Roybal et al., 2018) and both gene loci have SNP risk associations with PVR (Rojas et al., 2010; Sana-bria Ruiz-Colmenares et al., 2006). TNF- $\alpha$  has been found to activate TGF- $\beta$  expression (Takahashi et al., 2010), and therefore the combinatorial effects warrant further study. Receptors for TGF- $\beta$  and TNF- $\alpha$  are expressed on human native RPE cells (Strunnikova et al., 2010) and several studies document human RPE responses to these factors.

We found that TGF- $\beta$ 1 and TNF- $\alpha$  synergistically activate an EMT program in adult human RPE stem cell (RPESC)-RPE, producing fibroblastic, contractile membranes





(legend on next page)



*in vitro* resembling ERMs found in macular pucker and PVR. To characterize the process underlying this cellular transition, we comprehensively mapped the associated epigenetic and transcriptional changes. The most prominent epigenomic change accompanying RPE EMT was a gain of active chromatin marks at many putative enhancer elements. Correlating the epigenomic and transcriptomic data of TNT-treated RPE, we identified the landscape of gene regulation accompanying EMT, identifying several transcription factors (TFs) as candidate regulators of this process.

Previously, we reported that the TGF- $\beta$  pathway and inflammatory processes are significantly inhibited in human induced pluripotent stem cell-derived RPE treated with the vitamin B3 derivative nicotinamide (NAM) (Saini et al., 2017). Here, we demonstrate that NAM treatment of adult RPESC-RPE enhances the epithelial phenotype, prevents EMT, preserves RPE cell identity, and prevents the contractile behavior stimulated by combined TGF- $\beta$ 1 and TNF- $\alpha$  treatment (Schiff et al., 2019). Understanding the molecular changes accompanying RPE EMT and the impact of NAM has the potential to benefit patients with ERMs that contribute to vision loss.

## RESULTS

### Combined TGF- $\beta$ 1 and TNF- $\alpha$ Treatment Induces Adult Human RPESC-RPE to Undergo EMT

RPESCs were isolated and expanded from adult human cadaver globes, then differentiated into quiescent, polarized cobblestone monolayers (Blenkinsop et al., 2015; Fernandes et al., 2018) (Figure 1A). Adult RPESC-RPE cell cultures from three donors were treated with TGF- $\beta$ 1 alone, TNF- $\alpha$  alone, or their combination TGF- $\beta$ 1 + TNF- $\alpha$  (TNT), for 5 days. Treatment with either factor singly caused the RPE cells to transition from a cobblestone to a fibroblastic monolayer, while with the combined TNT treatment RPE cells acquired a more advanced mesenchymal phenotype and formed 3D aggregates (Figure 1B). Time-lapse movies capturing the dynamic changes occurring upon TNT treatment show increased motility and

apparent contractile behavior with 3D membrane-like formation (Video S1).

TNT treatment led to synergistic upregulation of the EMT master TFs *SNAI1*, *SNAI2*, and *TWIST1* (Figure 1C). *SNAI1* expression increased  $112.23 \pm 27.91$  (fold over control),  $p < 0.01$  ( $n = 3$ ), after TNT treatment but only  $7.89 \pm 2.21$ -fold,  $p < 0.05$  ( $n = 3$ ) after TGF- $\beta$ 1 alone and was similar to control after TNF- $\alpha$  alone. *SNAI2* expression increased  $36.08 \pm 6.31$ -fold,  $p < 0.01$  ( $n = 3$ ) upon TNT treatment, while TGF- $\beta$ 1 alone and TNF- $\alpha$  alone had little effect. *TWIST1* expression increased  $11.26 \pm 1.05$ -fold,  $p < 0.01$  ( $n = 3$ ) in TNT conditions compared with control, while treatment with TGF- $\beta$ 1 alone increased *TWIST1* expression by  $6.36 \pm 1.91$ -fold,  $p < 0.05$  ( $n = 3$ ) and TNF- $\alpha$  alone had negligible effect. The upregulation of nuclear localized SNAI1 protein in TNT conditions was confirmed by immunocytochemistry (Figure 1D).

We compared expression of genes characteristic of RPE (*MITF* and *BEST1*) and EMT (*SNAI1*) in 5-day TNT-treated versus vehicle-treated (control) RPE cells isolated from four different donors versus ERMs surgically removed from four different patients (Figures 1E and 1F). Patient-dissected ERMs expressed *MITF* at significantly lower levels:  $0.21 \pm 0.79$ ,  $p < 0.01$  ( $n = 4$ ) than control RPE (normalized to 1 for each sample), as did TNT-treated RPE  $0.055 \pm 0.023$ ,  $p < 0.01$  ( $n = 4$ ). *BEST1* expression in patient-dissected membranes varied widely  $19.48 \pm 14.47$ ,  $p > 0.05$  ( $n = 4$ ), and was not significantly different from control RPE or TNT-treated RPE  $2.63 \pm 2.63$ ,  $p > 0.05$  ( $n = 4$ ). *SNAI1* expression was significantly increased in patient-dissected membranes  $12.5 \pm 2.13$ ,  $p < 0.01$  ( $n = 4$ ), compared with control RPE, consistent with the high level of *SNAI1* expression in TNT-treated RPE ( $22.51 \pm 1.46$ ,  $p < 0.01$ ;  $n = 4$ ) and with previous findings in PVR tissue. Hence, TNT-treated RPE and patient-dissected ERMs have related morphological and gene expression changes, corroborating our previous studies (Schiff et al., 2019).

### TNT Induces Dynamic Changes in Enhancer Epigenetic Status

We performed chromatin immunoprecipitation (ChIP) for the histone marks H3K27ac, H3K4me3, and H3K4me1 and

### Figure 1. TGF- $\beta$ 1 + TNF- $\alpha$ Co-treatment (TNT) of RPESC-RPE Cells Induces EMT and Formation of *In Vitro* Membranes Similar to ERMs

- (A) Schematic of RPE isolation and *in vitro* ERM model generation.  
 (B) Phase images showing RPE cells in control conditions (cobblestone morphology) or 5 days after treatment with 10 ng/mL of TGF- $\beta$ 1, TNF- $\alpha$ , or both TGF- $\beta$ 1 + TNF- $\alpha$  (TNT).  
 (C) Time course (0, 1, 3, and 5 days) of *SNAI1*, *SNAI2*, and *TWIST1* expression in control RPESC-RPE cells (vehicle treated) and with 10 ng/mL of TGF- $\beta$ 1, TNF- $\alpha$ , or both (TNT),  $n = 3$  biological replicates.  
 (D) Immunofluorescence images of RPE cultures stained with anti-SNAI1 antibody show upregulation in TNT conditions.  
 (E) Fundus image of a patient with ERM (indicated by dotted line).  
 (F) RNA isolated from patient ERMs compared with *in vitro* RPE in control and TNT conditions assessed by qPCR for expression of RPE and EMT genes.  $n = 4$  biological replicates. Scale bars, 50  $\mu$ m. \*\* $p \leq 0.01$ .



identified enrichments across the genome; there was good correlation between replicates (e.g., Figure S1). When signal enrichments from control vehicle-treated cobblestone versus TNT-treated EMT RPE cells were compared, a major reorganization of H3K27ac and, to a lesser degree, H3K4me1 patterns upon EMT induction was apparent; interestingly, unlike many cell fate transitions that we have previously studied (Buecker et al., 2014) this EMT-associated reorganization is highly asymmetric with many more sites gaining H3K27ac (red) than losing (blue) or remaining unchanged (orange) (Figures 2A and 2B). This indicates that more regulatory elements become activated than are decommissioned upon TNT treatment (approximately 11,000 versus 4,000 at false discovery rate [FDR] < 0.1).

To investigate whether these changes correspond to epigenomic reorganization at enhancers or promoters, we analyzed the H3K4me1/H3K4me3 ratios and observed that regions that gain H3K27ac (e.g., identified as red in Figure 2A), tend to have a high H3K4me1/H3K4me3 ratio, suggestive of enhancer identity, whereas the regions that lose H3K27ac (blue) or remain unchanged (orange) are represented among both high and low H3K4me1/H3K4me3 ratio regions, indicating that they may harbor either promoter or enhancer activity (Figure 2C). Consistent with the notion that RPE EMT is associated with widespread enhancer activation, most regions with changes in H3K27ac were located more than 10 kb away from the nearest transcription start site (Figure 2D), as would be expected with long-range elements, such as enhancers.

Functional annotation of these dynamically changing, putative active enhancer regions by GREAT analysis revealed association of TNT-induced enhancers with arteriosclerosis, wound healing, growth factor activity, and cell growth and proliferation (Figure S2A), whereas regulatory regions that were downregulated by the TNT treatment were linked to retinal epithelium, RPE, visual perception, and retinal degeneration categories (Figure S2B). Regulatory regions found unchanged between control cobblestone RPE and TNT-treated RPE included both injury-related and neural development terms (Figure S2C). Altogether, we found that TNT treatment of RPE is associated with massive reorganization of epigenomic patterns, especially with the induction of thousands of new putative enhancer elements.

### Transcriptional Changes in RPE after TNT Treatment

Observed widespread epigenomic changes prompted us to investigate changes in gene expression that accompany TNT treatment of RPE. Using RNA from the same samples used in the ChIP sequencing (ChIP-seq) analysis, we performed RNA sequencing (RNA-seq) to examine the changes in transcription occurring due to TNT treatment (Table

S1A). To target more precisely the associated gene expression changes, we used EdgeR and DESeq packages to compare RNA-seq data from the four conditions: cobblestone RPE treated with vehicle (control) to TNF- $\alpha$  alone (Table S1B), TGF- $\beta$  alone (Table S1C), or both (TNT) (Table S1D). Compared with cobblestone RPE, 567 and 18 genes significantly changed after 5 days of treatment with TNF- $\alpha$  or TGF- $\beta$  alone, respectively, while a much larger number, 2,839 genes, changed significantly after TNT treatment, consistent with the synergistic effect of the two pathways (Table S1D) (FDR = 0.01). Kyoto Encyclopedia of Genes and Genomes (KEGG) pathway analysis of the genes upregulated in TNT indicates focal adhesion, ECM-receptor interaction, cytokine responses, and regulation of the actin cytoskeleton, fitting with observed changes in cell morphology, adhesion, and response to exogenous factors, while downregulated genes are primarily in metabolic pathways (Figures 3A and 3B; Tables S2A and S2B). Gene ontology enrichment analysis with the cateGOizer webtool (Na et al., 2014) gives a similar picture, with the fraction of terms associated with development, morphogenesis, differentiation, and cell signaling forming a larger fraction of the enriched terms in the TNT-treated compared with control RPE cells (Figures 3C and 3D; Tables S3A–S3D). We explored further the expression of TGF- $\beta$  and TNF- $\alpha$  receptors, confirming their expression in cobblestone RPESC-RPE and examining how the expression changed upon cytokine treatment by STRING analysis and qPCR (Figure S3). Interestingly, TGFBR2 increases after TNT treatment, while TGFBR3 decreases.

To examine the relationship between genes increased in TNT-treated RPE and other tissues undergoing EMT, we interrogated the dbEMT resource (<http://dbemt.bioinfo-minzhao.org/>), a manually curated database of genes experimentally verified to play a role in EMT across a variety of cancers and tissues (Zhao et al., 2015). Of the 344 genes in the dbEMT resource, 63 genes, approximately 20%, were also upregulated in RPE after TNT treatment, which is a strong enrichment (Fisher's exact test,  $p < 0.001$ ). Overall, the results of expression data analyses are consistent with changes in cell function and activity associated with the dramatic phenotypic changes that RPE cells undergo upon TNT treatment, and reveal both similarities with gene expression changes associated with EMT in other tissues and those more unique to RPE EMT.

### Integrating Transcriptional Changes Identifies RPE EMT-Related Genes

We then sought to understand the relationship between the epigenetic reorganization and changes in gene expression upon TNT treatment. We identified 12,516 unique genes closest to the 40,949 significantly changing regions based on H3K27ac marks (Table S1A), including 10,264 unique

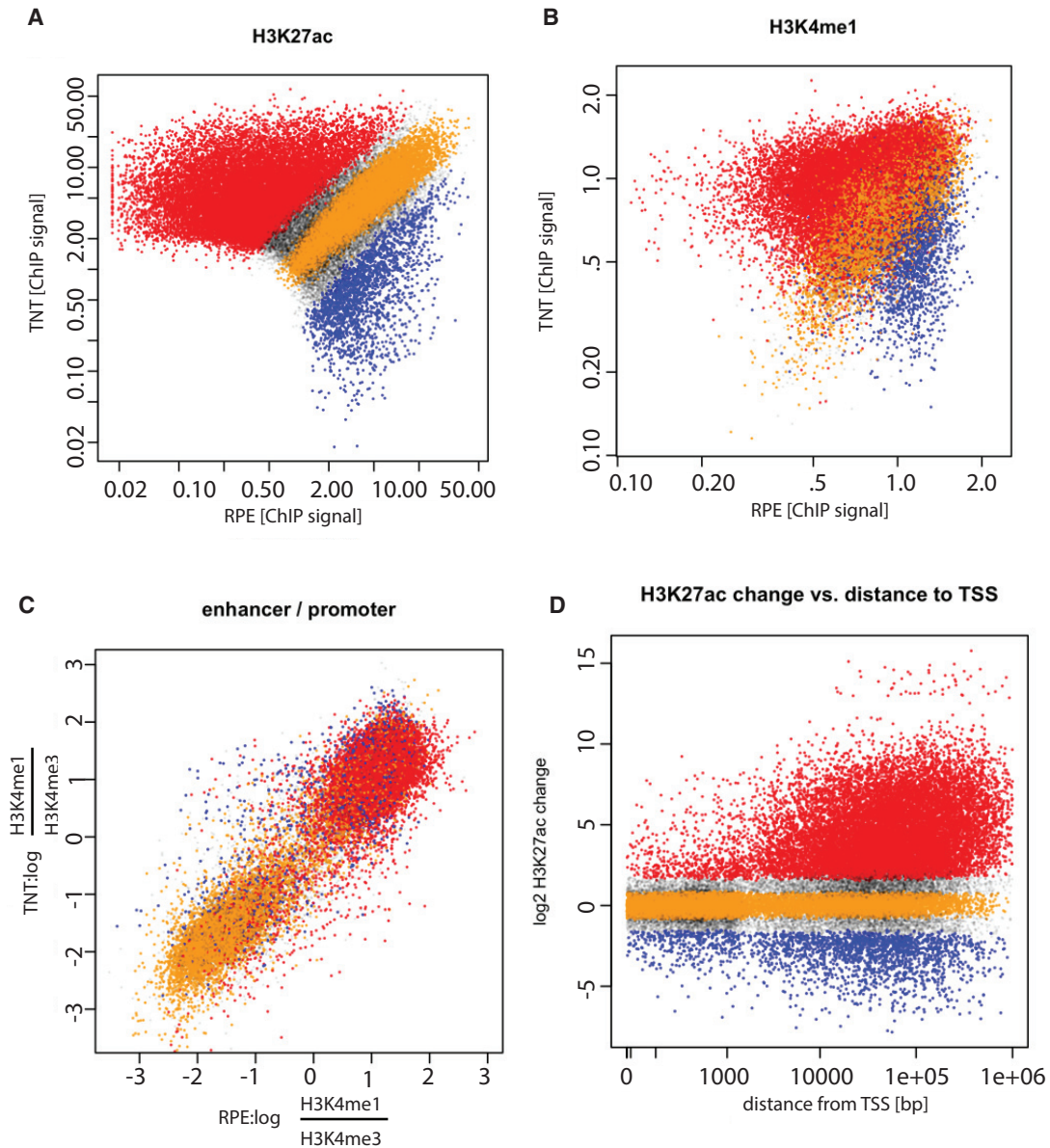


**Figure 2. TGF- $\beta$ 1 + TNF- $\alpha$  (TNT) Co-treatment of RPESC-RPE Cells Induces Global Epigenetic Changes at Enhancer Elements**

(A) TNT co-treatment induced changes in *H3K27ac* acetylation: abscissa—normalized read density of *H3K27ac* ChIP-seq at chromatin features (putative enhancers and promoters) in cobblestone RPE cells; ordinate—normalized read density of *H3K27ac* ChIP-seq in TNT-treated RPE cells. Regions in red have significantly upregulated ChIP signal upon TNT treatment (FDR < 0.01), in blue downregulated (FDR < 0.01), and in orange no change (FDR < 0.1).

(B) Changes in the *H3K4me1* ChIP signal are correlated with *H3K27ac* changes, regions color coded according to the *H3K27ac* classes defined in (A).

(C) TGF- $\beta$ 1 + TNF- $\alpha$  treatment results in relatively few changes in promoter signatures. Negative values indicate a promoter-like chromatin signature at interrogated sites. Color coding as in previous panels.

(D) Most changes in *H3K27ac* acetylation occur at sites distal from annotated transcription start sites. Plotted is the absolute distance to the closest annotated TSS versus the log<sub>2</sub> fold change in the *H3K27ac* ChIP signal: genes associated with distal elements with upregulated *H3K27ac* (red), downregulated *H3K27ac* (blue), or unchanged (orange). The differences are significant with p values indicated (Mann-Whitney-Wilcoxon test). n = 2 biological replicates.

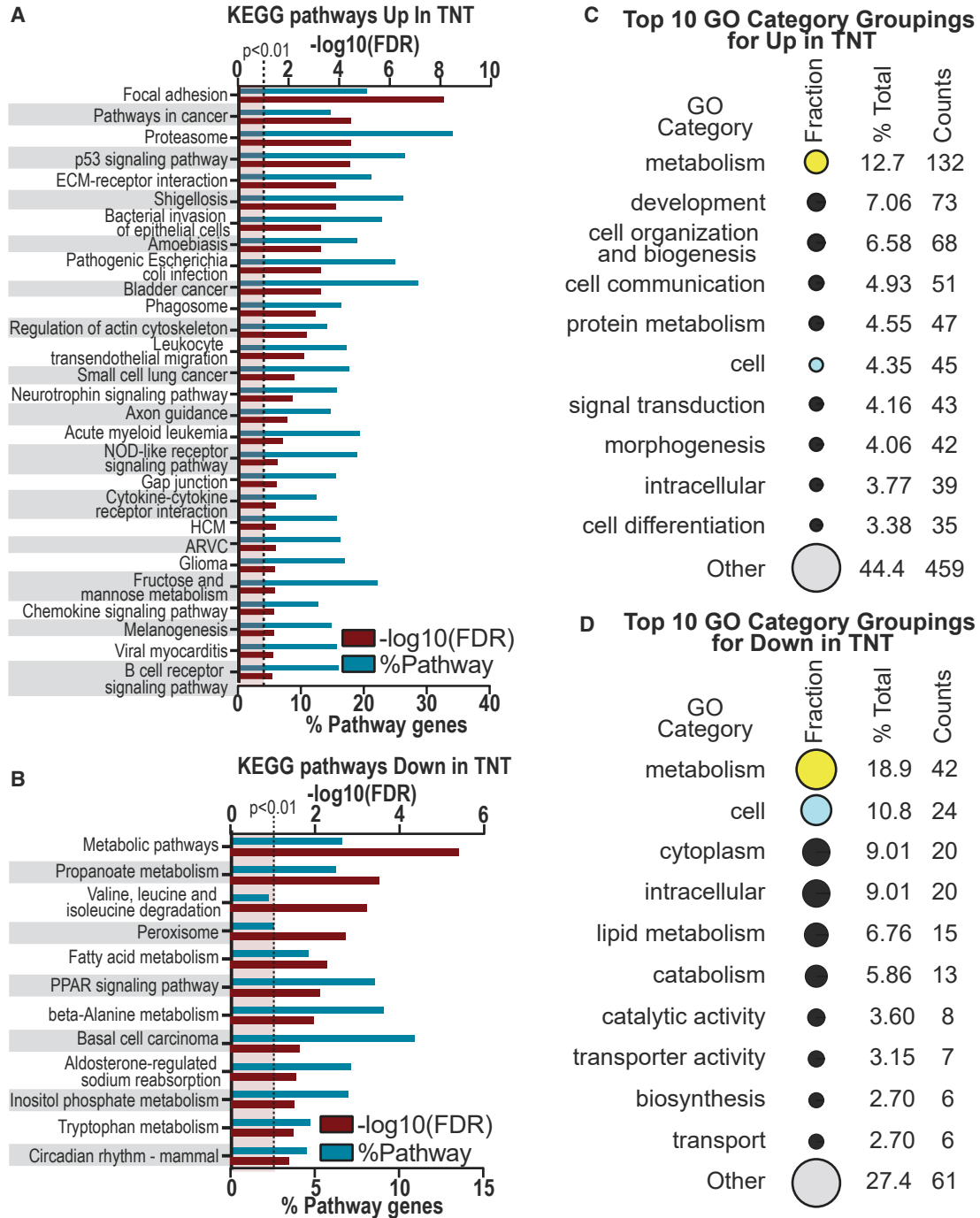


**Figure 3. RNA-Seq of RPE Undergoing TNT-Stimulated EMT Correlated with Epigenomic Changes**

(A and B) KEGG pathway enrichment analysis using the genes significantly upregulated (A) or downregulated (B) after TNT treatment (C and D) Gene ontology category analysis with goseq in combination with cateGOizer to classify and summarize the enrichment analysis revealed pathways enriched TNT-induced EMT RPE (C) and pathways enriched in cobblestone RPE (D). N = 2 biological replicates.

genes closest to the putative enhancer marks (Figure 4A). Of those genes with associated promoter or enhancer peaks, 2,293 genes also showed changes in expression in the RNA-seq analysis (Figure 4A), which represents ~80% of

the genes identified as changing. Broadly, regulatory elements that lose H3K27ac upon TNT treatment are associated with downregulated genes, and those that gain H3K27ac are associated with upregulated genes (Figure S4).

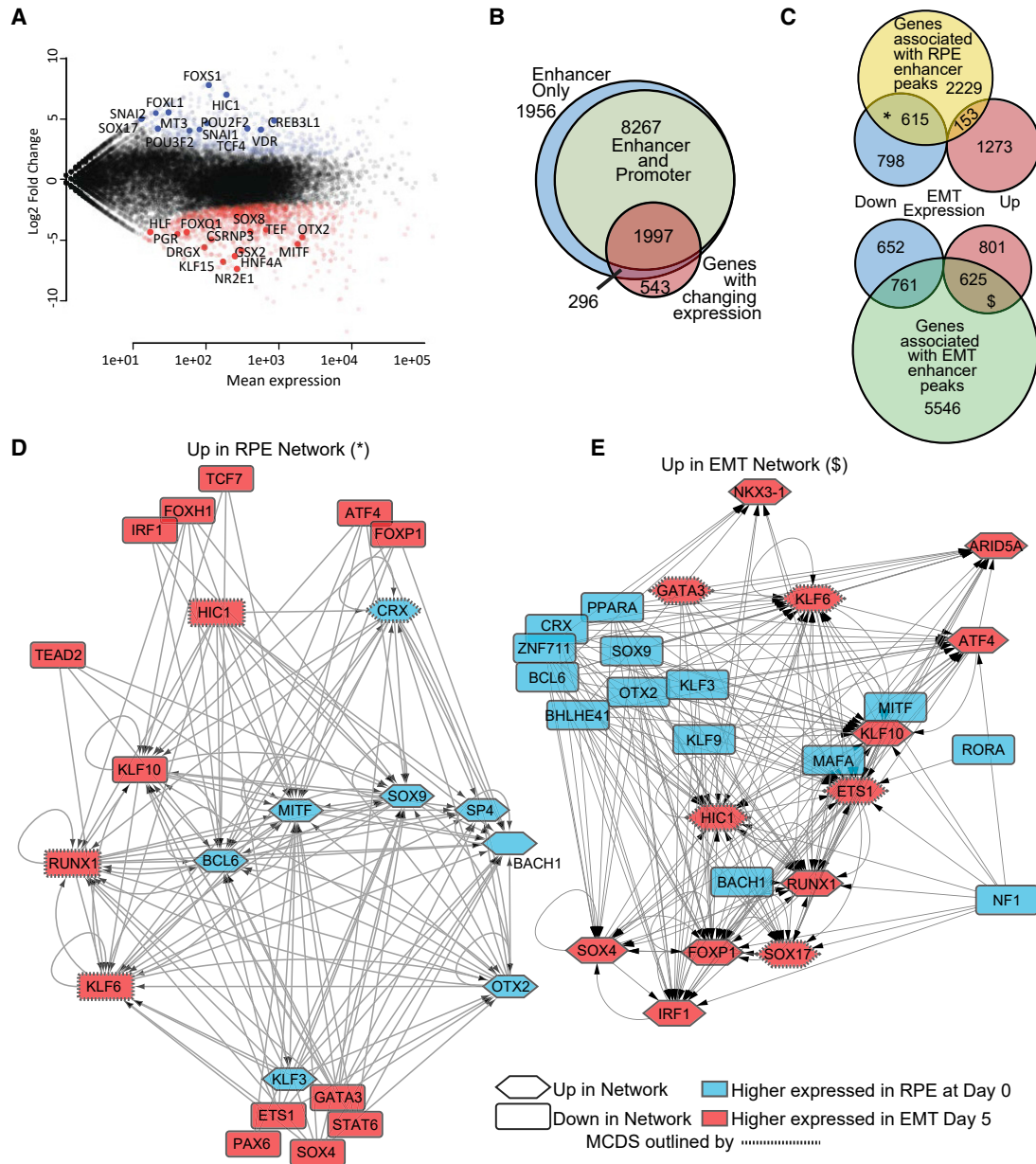


#### Figure 4. Integration of Transcriptional Changes and Epigenetic Changes during TNT-Induced EMT

(A) Scatterplot of expression changes after TNT treatment with selected transcription factors highlighted.

(B) Venn diagram showing the intersection between the differentially expressed genes and genes with either enhancer only or enhancer and promoter peaks.

(C) Venn diagrams of genes with significantly changing peaks in the cobblestone RPE (yellow) or with TNT-induced EMT RPE (green) overlapping with genes exhibiting increased (red) or decreased (blue) expression during EMT.

(D and E) Homer motif analysis of the subset of peaks and genes identified in (C) by \* (D) or \$ (E) identified key TFs potentially regulating the genes in each subset. Directed graphs based on the motif analysis were constructed and the minimum connecting dominating sets were identified. Shown are the subgraphs of the TFs for the RPE network (D) and the TNT network (E). Complete graphs and the motif analysis can be found at <http://neurosci.org/computing>.

In all, 2,997 and 6,932 genes were associated with enhancer peaks of different intensities in the RPE cobblestone and TNT conditions, respectively (Figure 4B). Of

the genes associated with more intense enhancer peaks in RPE cobblestone cells, 768 also changed expression after TNT treatment, with most decreasing. Of the genes



associated with more intense enhancer peaks after TNT treatment, 1,386 also changed expression: downregulated genes were again the majority, but the upregulated genes were more prominent compared with upregulated genes associated with RPE cobblestone peaks (625 [45%] versus 153 [20%] genes) (Figure 4C).

Although most changes occurred at distal enhancers, changes in epigenetic marks around the promoters of some significantly changing genes were also apparent. Of the 2,839 genes changing after TNT treatment, 1,997 also showed significant changes in the epigenetic marks near their promoters. For example, *INHBA*, *CO11A1*, and *TGF $\beta$ 1* molecules positively associated with EMT, showed upregulation of H3K4me1, and associated H3K27ac marks in promoter regions upon TNT treatment, while characteristic RPE genes, including *BEST1* and *RPE65*, showed reduction in these active promoter marks, changes also reflected in respective transcription levels (Figure S5; Table S1A). Together this analysis demonstrates a strong correspondence between the dynamic epigenetic and transcriptional changes we identified during TNT-induced EMT.

### Transcription Factor Changes Associated with RPE EMT

Considering the importance of TFs in binding to regulatory regions and executing gene expression changes, we evaluated which TFs may be involved in RPE EMT. Of the 2,839 genes that changed expression significantly between control cobblestone and TNT conditions, 424 were identified as likely TFs (GO:0006355, “regulation of transcription, DNA-templated”) (Table S4A). These include known master regulators of EMT, such as *SNAIL* and *SOX4* (Tiwari et al., 2013), and TFs more recently associated with EMT, such as *LMCD1* (Du et al., 2016), and several not previously associated, such as *FOXS1* (Figure 4A). Examination of histone marks in several of these TFs revealed expected changes reflecting their increased level of transcription, including increased H3K27ac at promoter regions (Table S1A). Conversely, RPE-associated TFs, such as *MITF* and *OTX2* showed lower expression levels in TNT versus RPE control conditions and overall reduced level of histone marks associated with transcriptional activity after TNT treatment (Table S1A).

To better understand the regulatory processes driving RPE EMT, we surveyed TF-binding motifs associated with peaks that changed and that were associated with significantly changing genes (Figure 4B). For this analysis, we examined peaks with differential intensity (adjusted p value < 0.1 and 2-fold change) between the RPE cobblestone and TNT conditions. For those peaks with a greater intensity in RPE cobblestone cells, we intersected the associated genes with the 1,413 genes that showed significantly decreased expression during EMT, resulting in 615 shared

genes (Figure 4C, subset marked by \*). For those peaks with a greater intensity in TNT-treated cells, we intersected the associated genes with the 1,426 genes that showed significantly increased expression during EMT, resulting in 625 shared genes (Figure 4C, subset marked by \$). For each case, we proceeded to uncover enriched TF consensus motifs in each subset by utilizing a motif analysis algorithm in the Homer suite of ChIP-seq tools (Heinz et al., 2010). Motif enrichment revealed a range of consensus sequences present within the RPE peak and EMT peak subsets (available at <http://neuralsci.org/computing>). In the RPE subset, 344 known motifs were enriched, and in the EMT subset, 324 known motifs were enriched ( $q < 0.1$ ). In both subsets the top ten motifs are against the same consensus sequences but in slightly different ranks. The Fra-1(bZip) motif is the top motif in both RPE and EMT peak subsets and it is promiscuous for the FOS family of TFs (*FOSL1*, *FOSL2*, *FOS*, and *FOSB*). We note that *FOSL1* exhibits a ~17-fold increased transcription during TNT-induced EMT. We then constructed directed networks for both the RPE cells and TNT-induced EMT cells of the changing genes and their potential regulators identified by the motif analysis. We first assigned interactions between the potential regulatory TFs and those genes with specific consensus motifs in their enhancer peaks that changed expression with EMT. The approach is somewhat lenient, in that all potential interactions were assumed to occur and added to the networks. One caveat of our approach is that broader motifs, such as E box, general AP-1, and the Fra-1 motifs, were not included due to their lack of specificity to a single TF. Hence, *FOSL1* is not included in the constructed networks, even though our analysis described above indicates it could be functionally important.

After constructing the networks, they were visualized in Cytoscape (v.3.6.1) (complete networks at <http://neuralsci.org/computing>) and the minimum dominating set (MDS) and minimum connected dominating set (MCDS) were determined using the MDCS plug-in (Nazarieh et al., 2016). The MDS and MCDS are algorithms for determining the key nodes in a network, in this case, the key TFs regulating a gene network. MDS identifies the minimum subset of nodes (subset A) such that every node not in A is directly adjacent to a node in A; MCDS identifies a similar subset with the caveat that all nodes in A must also be directly connected to each other. To focus on potential key regulatory genes and interactions in each complete network, we created subgraphs containing only the TFs that have changing expression and enriched consensus motifs (Figures 4D and 4E).

The complete “Up in RPE” network (Figure 4D is the TF subgraph) has 614 nodes (genes) with 8,466 edges (connections). In this network, the MCDS factors are *KLF6*, *CRX*, *HIC1*, and *RUNX1*, and the MDS is *KLF3* and *OTX2*. We



also created a subnetwork dropping TFs downregulated in RPE cobblestone cells as they undergo EMT, and in this case the MCDS factors are *BCL6*, *CRX*, *MITF*, *SOX9*, and *KLF9*, whereas the MDS factors are *CRX*, *SOX9*, and *KLF9*. *MITF* is a key TF in RPE development and function, and its inclusion as a central TF is expected, as is the case for *OTX2*, which directs the molecular network underlying RPE differentiation along with *MITF* (Martinez-Morales et al., 2003). *OTX2* expression drops by 26-fold in EMT RPE. The inclusion of *CRX* as a central factor in both the complete and subnetwork of Up in RPE is somewhat surprising given its well-established role in photoreceptor function and development, although it has been recognized more recently in RPE function in human and bovine retina (Esumi et al., 2009). *SOX9* is also important for RPE differentiation and in mature cells, *SOX9* regulates the key visual cycle genes (Masuda et al., 2014), explaining its significance in the Up in RPE network. It drops in expression by 6-fold in EMT RPE but retains prominence in the EMT network (Figure 4E), which is consistent with the known role that *SOX9* plays in the EMT of several cell types.

The complete “Up in EMT” network (Figure 4E is the TF subgraph) has 593 nodes and 8,890 edges and includes different central TFs. Examining this complete network, the MCDS factors are *KLF6*, *SOX17*, *GATA3*, *ETS1*, and *HIC1*, and the MDS factor is *KLF6*. In contrast to our findings on the Up in RPE network, the central TFs of the Up in EMT subnetwork (including only the TFs with increased expression in EMT) are not different from the complete network. Within both the Up in RPE and Up in EMT networks, KLF genes play a key role. Notably, *KLF6*, which increases in expression 2.6-fold after TNT treatment, is a central TF in both networks, and it has been demonstrated to have both repressor and activator activities. Antagonizing *KLF6* can inhibit TGF- $\beta$ -induced EMT (Limame et al., 2014). However, *KLF6* expression in kidney proximal tubule cells increased after EMT induction by TGF- $\beta$ , and *KLF6* overexpression promoted an EMT-like phenotype (Holian et al., 2008). These observations suggest a complex role for *KLF6* in EMT depending on tissue context or other transcriptional regulators.

### NAM Promotes a Cobblestone Phenotype, Improves Expression of RPE Markers, and Inhibits EMT in RPESC-Derived RPE

Inhibition of TGF- $\beta$  signaling can prevent loss of epithelial morphology (Kobayashi et al., 2019; Radeke et al., 2015; Zhang et al., 2018). Previously, we showed that NAM negatively regulates the TGF- $\beta$  signaling pathway and several genes associated with TNF- $\alpha$  signaling in RPE (Saini et al., 2017). In addition, NAM improves cobblestone phenotype in immortalized ARPE19 cells (Hazim et al., 2019). We found that, of the significantly changed genes in RPE

treated with NAM, remarkably, 47% (226) were also significantly changed upon TNT treatment (Table S4B), and most (155) in the opposite direction (Figures 5A and 5B; Table S4C). The TF *FOSL1*, which binds the top enriched consensus sequence in both the cobblestone and TNT-induced RPE cells, falls into this latter category. Furthermore, many of the gene ontology categories associated with genes upregulated by TNT treatment and downregulated by NAM treatment are shared (Figures 5C and 5D; Tables S4D and S4E). Hence, we hypothesized that NAM may inhibit EMT and the TNT-induced changes in RPE.

RPESC-RPE cultured without NAM had fibroblastic morphologies and appeared multilayered (Figures 6A and 6B, left panel), while those cultured with NAM were in a cobblestone monolayer (Figure 6B, right panel). The rate of change of transepithelial electrical resistance (TER) was compared between RPE cultured  $\pm$  NAM and slope of regression was calculated. NAM increased the TER of RPESC-RPE ( $320 \pm 32 \text{ cm}^2$ ,  $p = 1.61 \times 10^{-45}$ ,  $n = 9$ ) compared with no NAM ( $1.36 \pm 3.7$ ,  $p = 0.73$ ,  $n = 3$ ) (Figure 6C). Tight junction-associated proteins ZO-1 and CLDN19 appropriately localized to the apical membranes at cell-cell contacts in RPE cells cultured with NAM but were undetectable in cultures without NAM (Figure 6D). NAM promoted expression of key RPE identity markers *MITF* ( $1.72 \pm 0.18$ ,  $p = 0.0021$ ,  $n = 13$ ), *OTX2* ( $1.33 \pm 0.09$ ,  $p = 0.0146$ ,  $n = 6$ ), and *RPE65* ( $13.09 \pm 4.15$ ,  $p = 0.0141$ ,  $n = 12$ ) (Figure 6E). Western blot analysis showed that RPE cells cultured with NAM express more E- than N-cadherin, consistent with EMT inhibition (Figure 6F). Next, we examined expression of several key EMT and PVR-related genes by qPCR, including *SNAI1*, *SNAI2*, and *ACTA2* ( $\alpha$ -smooth muscle actin), which increases in expression during EMT as the cytoskeleton remodels. *COL1A1* encodes an extracellular matrix protein that is expressed in ERM tissue (Asato et al., 2013) and increases 9.6-fold after TNT treatment (Table S4). NAM decreased expression of *SNAI1* ( $0.41 \pm 0.05$ ,  $p = 0.0001$ ;  $n = 12$ ), *SNAI2* ( $0.50 \pm 0.05$ ,  $p = 0.0001$ ;  $n = 12$ ), and *ACTA2* ( $0.07 \pm 0.03$ ,  $p = 0.0016$ ;  $n = 3$ ) (Figure 6G). Hence, NAM effectively inhibits RPE EMT.

### NAM Restores Epithelial Identity by Promoting Mesenchymal-to-Epithelial Transition and Prevents Human RPE from Transforming into ERM-like Membranes In Vitro

Importantly, we found that NAM can promote a mesenchymal-to-epithelial transition (MET) in RPE cells. RPE which had already undergone EMT were cultured for 30 days  $\pm$  NAM (Figure 7A). NAM stimulated the reappearance of areas of cobblestone morphology (Figure 7B), increased expression of RPE identity genes, *MITF* ( $2.03 \pm 0.18$ ,  $p = 0.0054$ ;  $n = 5$ ) and *RPE65* ( $5.34 \pm 1.43$ ,  $p =$

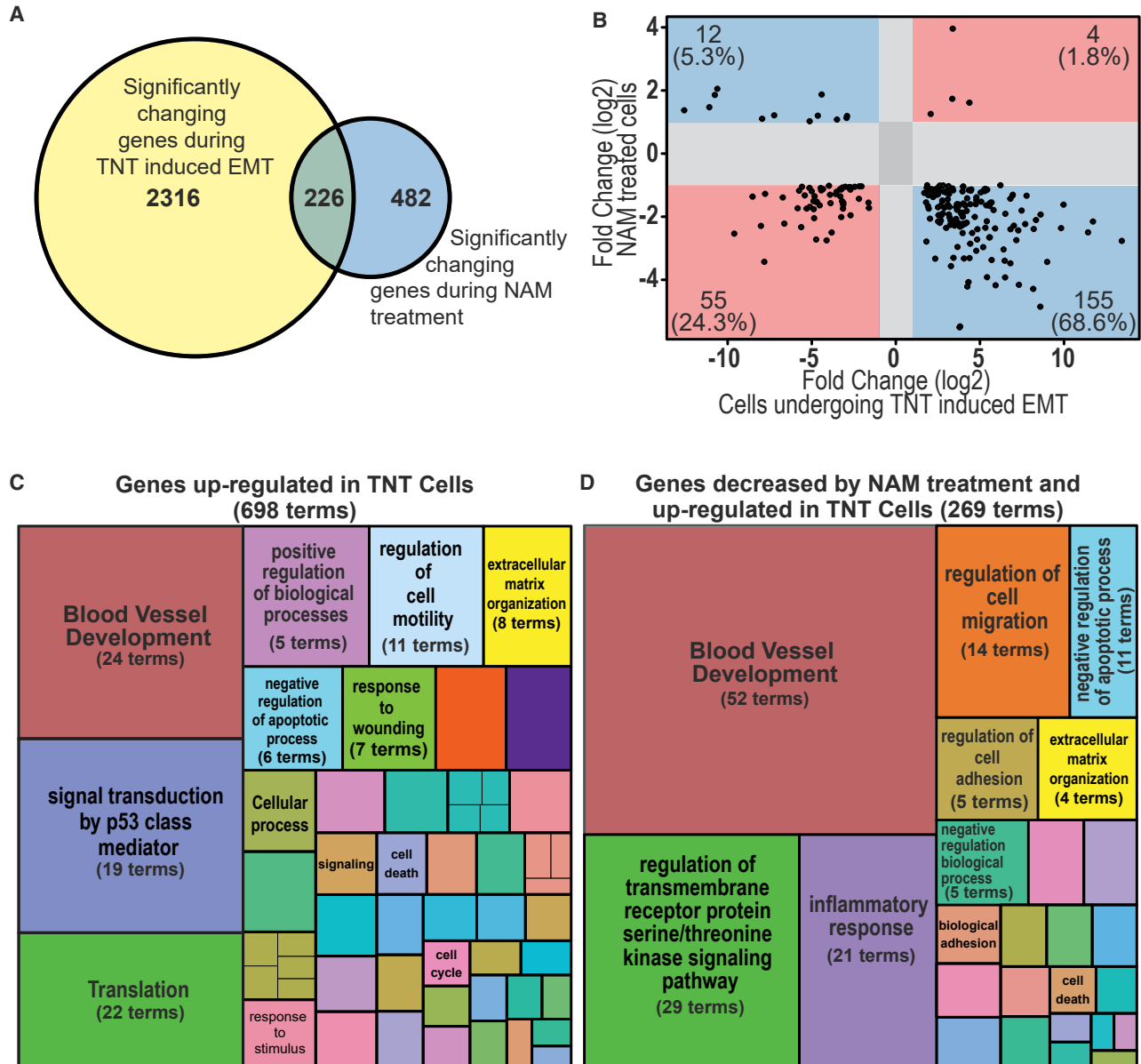


**Figure 5. Genes Changing Expression during TNT-Induced EMT versus Impact of NAM Treatment on Human RPE**

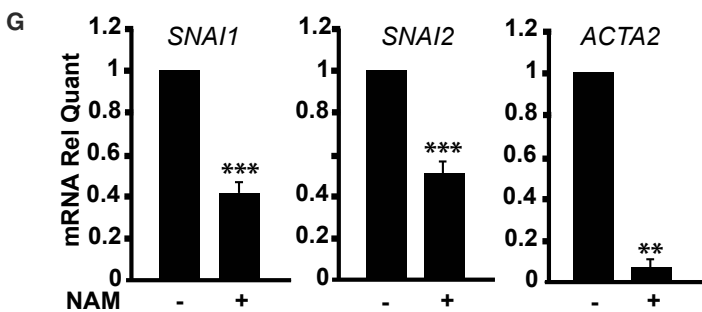
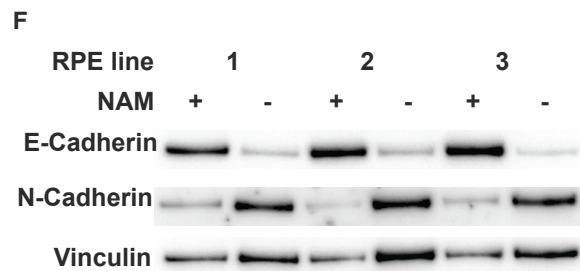
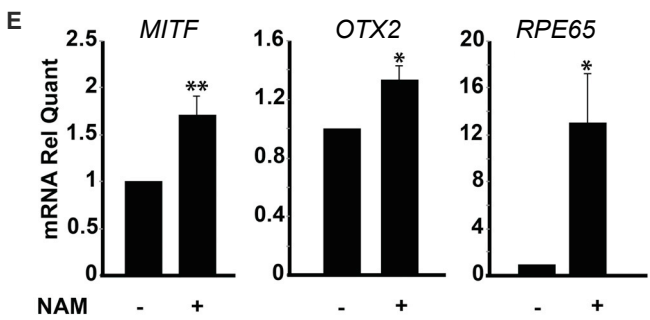
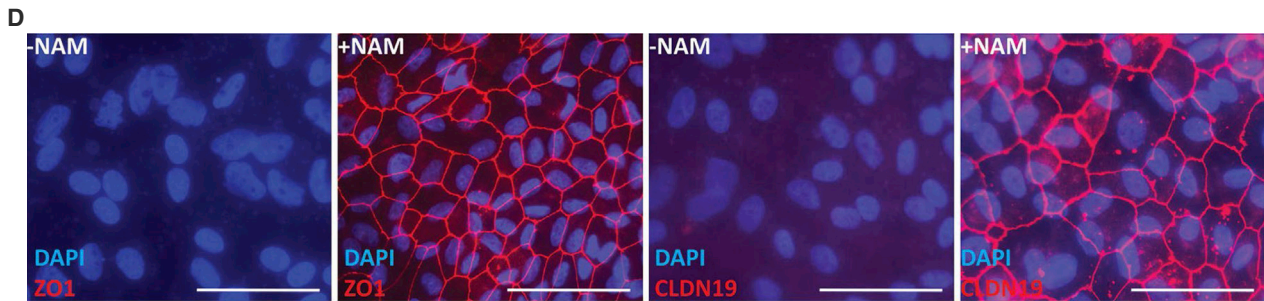
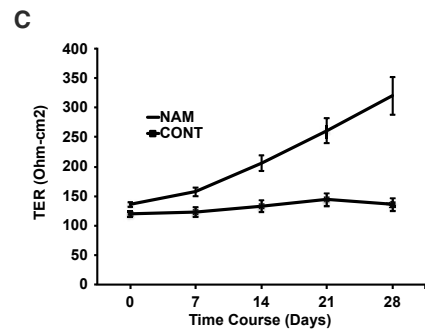
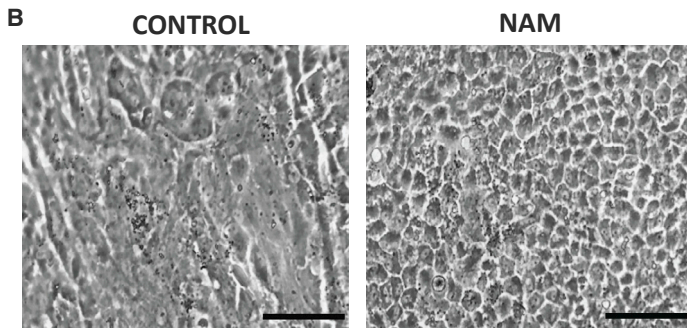
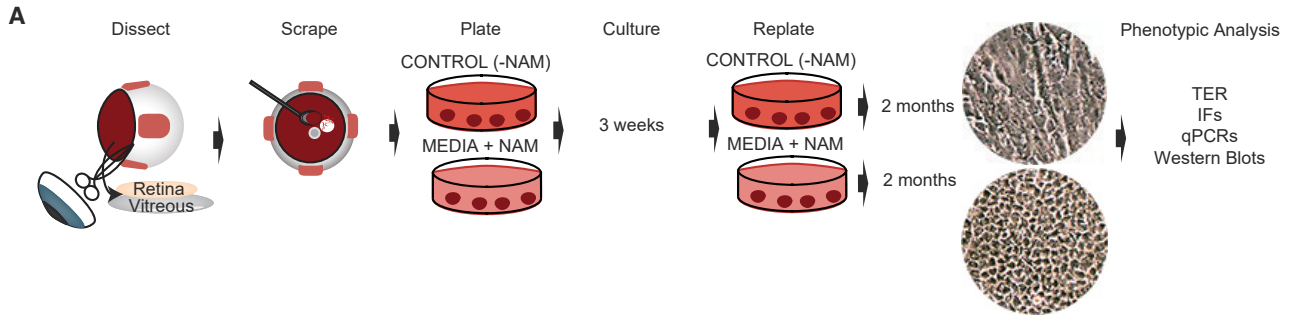
(A) RPE genes changing after NAM treatment and after TNT treatment.

(B) Scatterplot of the 226 genes significantly changed in RPE cells common to both NAM and TNT treatments. x axis: log<sub>2</sub> fold change after TNT treatment; y axis: log<sub>2</sub> fold change after NAM treatment. Lower right and upper left quadrants (blue boxes) contain genes whose expression in TNT is opposed by NAM treatment.

(C and D) Gene ontology enrichment analysis of gene categories aggregated based on semantic similarity using REVIGO and plotted as treemaps with top level descriptions, (C) genes upregulated during TNT-induced EMT, (D) genes from the lower right quadrant of (B). Comparison of the treemaps reveals similar strand enrichment for gene ontology categories related to blood vessel development, cell movement and adhesion, and apoptosis. Minor categories have been removed from treemap display to increase readability.

0.039; n = 5) (Figure 7C), and decreased expression of EMT-associated genes: *SNAI1* ( $0.33 \pm 0.17$ ,  $p = 0.0077$ ; n = 5) and *SNAI2* ( $0.19 \pm 0.03$ ,  $p = 0.0036$ ; n = 3) (Figure 7D). Furthermore, NAM treatment inhibited EMT stimulated by TNT (Figures 7E and 7F) (Video S2) and qPCR analysis showed

significantly reduced expression of EMT markers *SNAI1* ( $0.14 \pm 0.03$ ,  $p = 0.0002$ ; n = 3) and *SNAI2* ( $0.12 \pm 0.05$ ,  $p = 0.0005$ ; n = 3) (Figure 7G). To evaluate whether primary RPE may also form contractile membranes after TNT treatment, freshly isolated RPE cells were plated into TNT or





TNT + NAM conditions. Given that, by single-cell analysis, primary RPE cells that are largely post-mitotic (Salero et al., 2012), and the proliferative RPESCs are a minor subpopulation (<10%), we predicted only a low level of mass formation that would be inhibited by NAM treatment, which is what we observed (Figures 7H and 7I). These data demonstrate that NAM can prevent TNT-induced contractility and partially reverse the EMT phenotype in adult human RPESC-RPE cells in a model of PVR.

## DISCUSSION

Human RPE cells undergo pathological changes, including EMT, leading to conditions that can significantly impair vision. Treatment with TNT is a strong inducer of several changes seen in ERM and PVR formation, including EMT and production of contractile membranes, and here we investigated the global transcriptomic and epigenomic changes associated with these dramatic changes in RPE cells. Furthermore, we found that the vitamin B3 derivative NAM inhibits RPE EMT and prevents the formation of contractile fibroblastic membranes that resemble the damaging ERMs found in macular pucker and PVR.

TNT treatment resulted in widespread changes in the RPE epigenome, with an unusual bias toward activation of regulatory elements, rather than decommissioning. These changes in active chromatin signatures occurred largely at distal enhancers, while promoters were less affected. This is consistent with enhancers serving as the primary mediators of RPE cell state change and being utilized in a highly dynamic manner. H3K27ac enrichment at enhancers shows a high degree of cell type specificity and responsiveness to signaling (Calo and Wysocka, 2013); therefore, the changes we observe at putative enhancers are consistent with the RPE undergoing a drastic change in regulatory programs in response to these changes in the signaling environment.

Global epigenomic changes associated with EMT have been assessed in other cell types. In a mouse hepatocyte cell line treated with TGF- $\beta$  treatment to stimulate EMT, a striking loss of heterochromatin was observed, with a global reduction in the heterochromatin mark H3K9Me2,

an increase in H3K4Me3 and an increase in the transcriptional mark H3K36Me3 (McDonald et al., 2011). Immortalized human mammary epithelial cells stimulated to undergo EMT by overexpression of *TWIST1* showed an increase in H3K4me3 and dramatic reduction in the repressive mark H3K27me3, with loss at half of the gene promoters (Malouf et al., 2013). Human lung A549 alveolar epithelial cells treated with TGF- $\beta$  to stimulate EMT, however, produced no overall detectable change in global H3K4me3 levels but exhibited a global loss of the active euchromatin mark H3K9ac and an increase in the repressive mark H3K27me3 (Malouf et al., 2013). These different observations may be attributable to different methodologies, the mode of EMT induction, time points of assessment, and to the specific cell types involved. We note again that, since enhancers are often characterized by high cell-type specificity, the specific regulatory enhancer elements utilized for their activation may be different in distinct epithelial cell types. Thus, it will be valuable to determine whether the massive reorganization of enhancer patterns we observed in RPE also accompanies EMT in other cell types and whether the activated enhancers are overlapping or distinct. Associations between EMT-associated TFs and epigenetic regulatory machinery provide plausible routes to alterations in DNA methylation and histone modifications (Skrypek et al., 2017) that may have cell-specific outcomes and raise the importance of documenting these changes at molecular levels in diverse tissues and, where possible, with unified approaches to enable more precise comparisons.

Because TNT treatment elicited changes in over 40,000 identified epigenetic regions, we used global transcriptomics and differential gene expression analysis to reveal genes that exhibited concerted epigenetic and transcriptional changes. RNA-seq analysis identified genes that demonstrated expression changes between cobblestone and TNT conditions revealing associations with pathways known to be predominant in EMT. Acquisition of contractile properties is prominent after TNT treatment and represents the potentially damaging maturation of ERMs, so it is interesting that several genes associated with smooth muscle contraction, including *MYL9*, *MYL6*, the non-muscle

### Figure 6. NAM Protects RPESC-RPE Cells from Undergoing EMT

(A) Schematic of RPESC-RPE culture procedure and analysis.

(B) Phase images of adult human RPESC-RPE cultures without (CONTROL) and with NAM. Scale bars, 100  $\mu$ m.

(C) TER measurements of adult human RPE cultured without (CONT) and with NAM. N = 3 biological replicates.

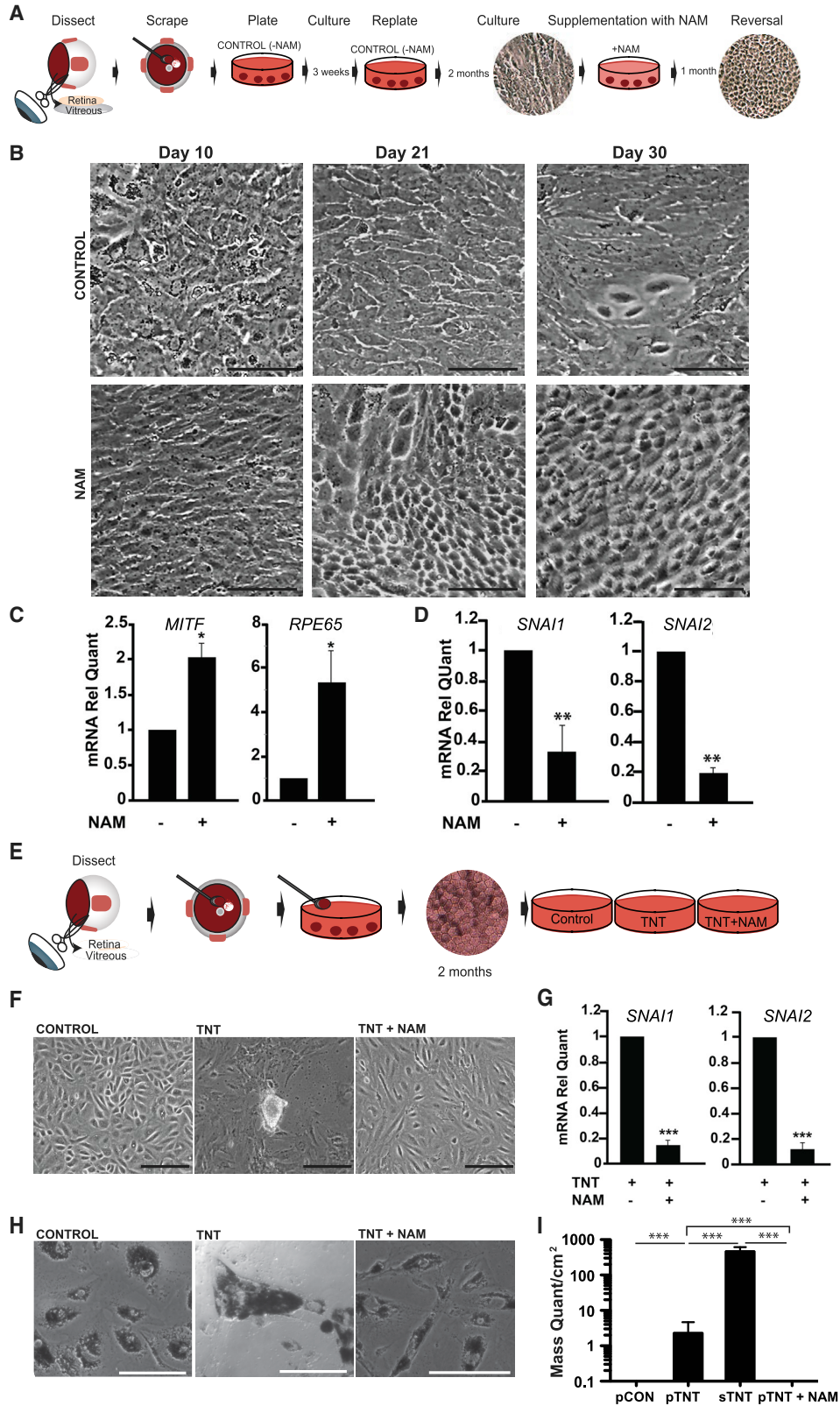
(D) Immunofluorescence images of ZO-1 and CLDN19 (red) after 1 month in culture with NAM (nuclear stain, DAPI, blue). Scale bars, 100  $\mu$ m.

(E) qPCR for RPE identity genes *MITF*, *OTX2*, and *RPE65*. N = 12 biological replicates.

(F) Western blot analysis for E- and N-cadherin in three adult human RPE lines; vinculin as loading control.

(G) qPCR analysis of EMT master regulator genes (*SNAI1* and *SNAI2*) and EMT marker (*ACTA2*).

All values are relative to control without NAM (–). \*p < 0.05, \*\*p < 0.01, \*\*\*p < 0.001; n = 3 biological replicates.



(legend on next page)



myosin *MYH9*, and several tropomyosin genes, are significantly upregulated, and targeting these may reduce the impact of pulling and detaching retinal tissue.

Comparison of the significantly changing genes between cobblestone and TNT-treated RPE and association with putative active enhancers and promoters in our analysis revealed several TFs that are candidate regulators of RPE EMT. In addition to the canonical EMT factors, and those already described through a network analysis focused on ARPE19 cells (Pratt et al., 2008), several have not been explored in the context of RPE EMT and ERM development, such as *KLF6*, *SOX17*, and *FOSL1*. It will be worthwhile to examine whether such TFs highlighted by our network analyses are involved in the initiation of ERM production and contraction during progression of macular pucker and PVR. Our observations that NAM inhibits RPE EMT and moreover can initiate MET, opens opportunities to develop deeper insight into the processes involved, and a pathway to new therapeutic approaches for clinical conditions subsequent to RPE EMT, including ERM, macular pucker and PVR.

## EXPERIMENTAL PROCEDURES

### Human Adult RPESC-RPE Culture

Human whole globes and posterior shells (globes without anterior segments) from donors aged 36–90 years within 40 h of death were obtained from the National Disease Research Interchange, Philadelphia, PA, the Eye-Bank for Sight Restoration, New York, NY, the Lions Eye Bank, Albany, NY, and Miracle In Sight, Winston-Salem, NC. Eye dissection and culture protocols were as published (Blenkinsop et al., 2013; Fernandes et al., 2018). RPE cells were isolated and plated on tissue culture plates coated with Synthemax II (Corning) in RPE medium with 10% fetal bovine serum (FBS) and 10 mM NAM and fed 3 times a week; after the first week, FBS was reduced to 2%.

### Patient-Dissected ERM Specimens

Specimens were obtained within 24 h of surgery at the New York Eye and Ear Infirmary (Mount Sinai Hospital, NY) and Capitol Region Retina (Albany, NY) and were immediately processed for RNA extraction and qPCR analysis. Statistical analysis was conducted using Student's t test. Studies were conducted under IRB oversight.

### EMT Model

Human RPESC-RPE cultures were treated with 0.25% trypsin for 5 min, washed and replated at  $3 \times 10^4$  cells per  $1.9 \text{ mm}^2$  in a 24-well plate in DMEM/F12 + 5% FBS, L-glutamine, Na-pyruvate, non-essential amino acid, penicillin/streptomycin. After 24 h, 10 ng/mL TGF- $\beta$ 1 or 10 ng/mL TNF- $\alpha$ , or 10 ng/mL of each (TNT) were added versus vehicle as control, and cultures were fed every other day for 5 days.

### Immunohistochemistry and Western Blot

Adult human RPESC-RPE on 24-well size Transwell inserts (Corning) were fixed with 4% paraformaldehyde for 10 min, rinsed 3 $\times$  with phosphate-buffered saline, permeabilized with 0.02% Tween 20, and blocked with normal goat or donkey serum (5%) in BSA (1%) for 1 h. Primary antibodies against SNAI1 (goat, diluted 1:100, R&D Systems, cat. no. AF3639), Z-O1 (mouse, diluted 1:100, Invitrogen, cat. no. 339100), and CLDN19 (rabbit, diluted 1:100, Abcam, cat. no. ab74374) were added, incubated overnight at 4°C, then washed and incubated for 45 min at room temperature with the corresponding Alexa Fluor-conjugated secondary antibodies (1:1,000) (Life Technologies Alexa Fluor 488 donkey anti-goat IgG [H + L], cat. no. A11055; Alexa Fluor 488 goat anti-mouse IgG [H + L], cat. no. A11017; Life Technologies Alexa Fluor 488 donkey anti-rabbit IgG [H + L], cat. no. A11070). DAPI (Roche, cat. no. 10-236-276-001) was added at room temperature for 45 min as a nuclear counterstain. Cells on Transwell inserts were mounted on glass slides with Prolong Gold (Life Technologies, cat. no. P36930) and imaged by fluorescent microscopy (Leica DM5500). Western blot methods are provided in [Supplemental Information](#).

### RNA Isolation and qPCR

Adult human RPESC-RPE cells were incubated in RNAprotect Cell Reagent (QIAGEN, cat. no. 76,526), centrifuged at 10,000 rpm for 10 min, and the pellet resuspended in buffer RLT plus and RNA harvested according to the manufacturer's protocol (QIAGEN RNeasy Plus Mini Kit, cat. no. 74,136). Samples were passed through a gDNA eliminator column (QIAGEN). cDNA was made using the high-capacity RNA to cDNA conversion kit (Applied Biosystems, cat. no. 4387406). qPCR was performed using Radiant Green Lo-ROX qPCR Kit (Alkali, cat. no. QS1020) and Applied Biosystems ViiA7 Real-Time PCR System (Life Technologies). qPCR primers are provided in [Supplemental Information](#). Statistical analysis was conducted using Student's t test.

## Figure 7. NAM Promotes RPESC-RPE MET and Inhibits 3D ERM-like Membrane Formation

- (A) Schematic of experiment to determine if NAM can stimulate MET.  
 (B) Phase images of RPE cultures showing NAM treatment restores cobblestone morphology, scale bars, 100  $\mu\text{m}$ .  
 (C and D) qPCR analysis for (C) RPE identity genes *MITF* and *RPE65*, and (D) EMT master genes *SNAI1* and *SNAI2*. N = 5 biological replicates.  
 (E) Schematic of experiment to determine if NAM can prevent TNT-induced changes in adult RPESC-RPE cultures.  
 (F) Phase images of cultured adult human RPE cells after 5 days of culture in CONTROL (Vehicle), TNT, or TNT + NAM. Scale bars, 100  $\mu\text{m}$ .  
 (G) qPCR analysis of EMT master genes *SNAI1* and *SNAI2*. N = 3 biological replicates.  
 (H) Phase images of primary adult human RPE after 5 days in culture in CONTROL (Vehicle), TNT, or TNT + NAM. Scale bars, 100  $\mu\text{m}$ .  
 (I) Quantification of number of 3D masses produced primary RPE with vehicle control (pCON), primary RPE treated with TNT (pTNT), RPESC-RPE (sTNT), primary RPE treated with TNT + NAM (pTNT + NAM). N = 3 biological replicates.  
 \*p < 0.05, \*\*p < 0.01, \*\*\*p < 0.001.



## ChIP-Seq

ChIP assays were performed from  $\sim 10^7$  RPESC-RPE cells per experiment, across two different donors, according to (Rada-Iglesias et al., 2011), with slight modification; further details in [Supplemental Information](#). Functional annotation of enhancers was obtained with GREAT (<http://great.stanford.edu/public/html/input.php>), using the Basal plus extension association rules and the whole human genome as background.

## RNA-Seq

RPESC-RPE cells from two different donors were treated with TGF- $\beta$ 1 TNF- $\alpha$ , TNT, or vehicle control as described above for 5 days. RNA was extracted with TRIzol (Invitrogen) following THE manufacturer's recommendations. Total RNA (10  $\mu$ g) underwent two rounds of purification using Dynaloligo-dT beads (Invitrogen), was fragmented with 10 $\times$  fragmentation buffer (Ambion), and used for first-strand cDNA synthesis using random hexamer primers (Invitrogen) and SuperScript II enzyme (Invitrogen). Double-strand cDNA was obtained by adding RNaseH (Invitrogen) and DNA Pol I (New England BioLabs) and used for Illumina library preparation and sequenced with the Illumina HiSeq.

## Transepithelial Resistance Measurements

Transepithelial resistance (TER) of RPESC-RPE cells grown in Transwell inserts (Corning)  $\pm 10$  mM NAM in RPE medium was measured weekly and within 2 min of removal from the incubator using an EVOM2 (World Precision Instruments) Epithelial VoltOhmmeter. Statistical analysis was conducted using Student's t test.

## Bioinformatic Analysis

### ChIP-Seq

To identify the approximate positions of regulatory elements from histone modification ChIP-seq profiles alone, we calculated kernel density estimate tracks with bimodal kernels (Buecker et al., 2014) and identified peaks in the product of the combined H3K27 and H3K4 signals. To analyze changes in histone modifications, we calculated the read coverage for each sample over a combined set of detected peaks and performed a differential analysis with DESeq2.

### RNA-Seq

Fastq files were mapped using STAR aligner with the NCBI26/hg18 genome to generate bam files. Reads per genes were counted and read into R using the GenomicRanges package. Significantly changing genes were identified using the edgeR and DESeq2 packages. Gene ontology and KEGG enrichment analysis was performed with the goseq package.

Integration of ChIP-seq and RNA-seq data: was done in R and with Homer ChIP-seq toolset. For the network analysis, adjacency lists were generated in R and network visualization in Cytoscape 3.5. The MCDS and MDS analysis was done with the MCDS Cytoscape app. See [Supplemental Information](#) for R code and more details. REVIGO (<http://revigo.irb.hr/>) was used to generate treemaps for the gene ontology analysis.

## ACCESSION NUMBERS

All raw data are available upon request. Sequencing data have been deposited on <https://www.ncbi.nlm.nih.gov/geo/subs/>

, accession number GSE128144. All codes generated by the Temple lab are available at [https://github.com/neural-stem-cell-institute/RPE\\_EMT](https://github.com/neural-stem-cell-institute/RPE_EMT).

## SUPPLEMENTAL INFORMATION

Supplemental Information can be found online at <https://doi.org/10.1016/j.stemcr.2020.03.009>.

## AUTHOR CONTRIBUTIONS

S.T., J.W., T.A.B., M.F., and J.H.S. conceived the experiments and contributed to data analysis, interpretation and manuscript writing. A.R.-I., R.S., L.S., Q.W., J.S.S., T.A.B., M.F., and T.S. performed the experiments, made figures, and helped with manuscript preparation. T.S., T.K., and N.C.B. analyzed epigenomic and transcriptomic data and performed bioinformatic analyses.

## ACKNOWLEDGMENTS

We thank Dr. Barbara Corneo for manuscript review, Carol Charniga for invaluable help with eye dissection and cell culture, and the eye donors and their families. This study was supported by the National Eye Institute (NEI), Bethesda, MD, USA, extramural grant NEI 01EY022079 (to S.T.); the Empire State Stem Cell Fund through New York State Department of Health contract no. C028504 (to S.T. and J.H.S.); the Regenerative Research Foundation; the Macula Vision Research Foundation; and the Icahn School of Medicine at Mount Sinai (to T.A.B.). Opinions expressed here are solely those of the authors and do not necessarily reflect those of the Empire State Stem Cell Board, the New York State Department of Health, or the State of New York. J.H.S., S.T., and T.A.B. have a patent pertaining to discoveries presented in this manuscript. Patent no: 20150148383.

Received: May 3, 2019

Revised: March 8, 2020

Accepted: March 9, 2020

Published: April 2, 2020

## REFERENCES

- Asato, R., Yoshida, S., Ogura, A., Nakama, T., Ishikawa, K., Nakao, S., Sassa, Y., Enaida, H., Oshima, Y., Ikeo, K., et al. (2013). Comparison of gene expression profile of epiretinal membranes obtained from eyes with proliferative vitreoretinopathy to that of secondary epiretinal membranes. *PLoS One* 8, e54191.
- Blenkinsop, T.A., Saini, J.S., Maminishkis, A., Bharti, K., Wan, Q., Banzon, T., Lotfi, M., Davis, J., Singh, D., Rizzolo, L.J., et al. (2015). Human adult retinal pigment epithelial stem cell-derived RPE monolayers exhibit key physiological characteristics of native tissue. *Invest. Ophthalmol. Vis. Sci.* 56, 7085–7099.
- Blenkinsop, T.A., Salero, E., Stern, J.H., and Temple, S. (2013). The culture and maintenance of functional retinal pigment epithelial monolayers from adult human eye. *Methods Mol. Biol.* 945, 45–65.
- Buecker, C., Srinivasan, R., Wu, Z., Calo, E., Acampora, D., Faial, T., Simeone, A., Tan, M., Swigut, T., and Wysocka, J. (2014).



- Reorganization of enhancer patterns in transition from naive to primed pluripotency. *Cell Stem Cell* *14*, 838–853.
- Calo, E., and Wysocka, J. (2013). Modification of enhancer chromatin: what, how, and why? *Mol. Cell* *49*, 825–837.
- Du, L., Yamamoto, S., Burnette, B.L., Huang, D., Gao, K., Jamshidi, N., and Kuo, M.D. (2016). Transcriptome profiling reveals novel gene expression signatures and regulating transcription factors of TGFbeta-induced epithelial-to-mesenchymal transition. *Cancer Med.* *5*, 1962–1972.
- Esumi, N., Kachi, S., Hackler, L., Jr., Masuda, T., Yang, Z., Campochiaro, P.A., and Zack, D.J. (2009). BEST1 expression in the retinal pigment epithelium is modulated by OTX family members. *Hum. Mol. Genet.* *18*, 128–141.
- Fernandes, M., McArdle, B., Schiff, L., and Blenkinsop, T.A. (2018). Stem cell-derived retinal pigment epithelial layer model from adult human globes donated for corneal transplants. *Curr. Protoc. Stem Cell Biol.* *45*, e53.
- Girard, P., Mimoun, G., Karpouzas, I., and Montefiore, G. (1994). Clinical risk factors for proliferative vitreoretinopathy after retinal detachment surgery. *Retina* *14*, 417–424.
- Hazim, R.A., Volland, S., Yen, A., Burgess, B.L., and Williams, D.S. (2019). Rapid differentiation of the human RPE cell line, ARPE-19, induced by nicotinamide. *Exp. Eye Res.* *179*, 18–24.
- Heinz, S., Benner, C., Spann, N., Bertolino, E., Lin, Y.C., Laslo, P., Cheng, J.X., Murre, C., Singh, H., and Glass, C.K. (2010). Simple combinations of lineage-determining transcription factors prime cis-regulatory elements required for macrophage and B cell identities. *Mol. Cell* *38*, 576–589.
- Holian, J., Qi, W., Kelly, D.J., Zhang, Y., Mreich, E., Pollock, C.A., and Chen, X.M. (2008). Role of Kruppel-like factor 6 in transforming growth factor-beta1-induced epithelial-mesenchymal transition of proximal tubule cells. *Am. J. Physiol. Ren. Physiol.* *295*, F1388–F1396.
- Kalluri, R., and Weinberg, R.A. (2009). The basics of epithelial-mesenchymal transition. *J. Clin. Invest.* *119*, 1420–1428.
- Kita, T., Hata, Y., Arita, R., Kawahara, S., Miura, M., Nakao, S., Mochizuki, Y., Enaida, H., Goto, Y., Shimokawa, H., et al. (2008). Role of TGF-beta in proliferative vitreoretinal diseases and ROCK as a therapeutic target. *Proc. Natl. Acad. Sci. U S A* *105*, 17504–17509.
- Kobayashi, M., Tokuda, K., Kobayashi, Y., Yamashiro, C., Uchi, S.H., Hatano, M., and Kimura, K. (2019). Suppression of epithelial-mesenchymal transition in retinal pigment epithelial cells by an MRTF-A inhibitor. *Invest. Ophthalmol. Vis. Sci.* *60*, 528–537.
- Korthagen, N.M., van Bilsen, K., Swagemakers, S.M., van de Peppe, J., Bastiaans, J., van der Spek, P.J., van Hagen, P.M., and Dik, W.A. (2015). Retinal pigment epithelial cells display specific transcriptional responses upon TNF-alpha stimulation. *Br. J. Ophthalmol.* *99*, 700–704.
- Limame, R., Op de Beeck, K., Lardon, F., De Wever, O., and Pauwels, P. (2014). Kruppel-like factors in cancer progression: three fingers on the steering wheel. *Oncotarget* *5*, 29–48.
- Machemer, R. (1977). Massive periretinal proliferation: a logical approach to therapy. *Trans. Am. Ophthalmol. Soc.* *75*, 556–586.
- Machemer, R. (1988). Proliferative vitreoretinopathy (PVR): a personal account of its pathogenesis and treatment. Proctor lecture. *Invest. Ophthalmol. Vis. Sci.* *29*, 1771–1783.
- Malouf, G.G., Taube, J.H., Lu, Y., Roysarkar, T., Panjarian, S., Estecio, M.R., Jelinek, J., Yamazaki, J., Raynal, N.J., Long, H., et al. (2013). Architecture of epigenetic reprogramming following Twist1-mediated epithelial-mesenchymal transition. *Genome Biol.* *14*, R144.
- Martinez-Morales, J.R., Dolez, V., Rodrigo, I., Zaccarini, R., Leconte, L., Bovolenta, P., and Saule, S. (2003). OTX2 activates the molecular network underlying retina pigment epithelium differentiation. *J. Biol. Chem.* *278*, 21721–21731.
- Masuda, T., Wahlin, K., Wan, J., Hu, J., Maruotti, J., Yang, X., Iacovelli, J., Wolkow, N., Kist, R., Dunaief, J.L., et al. (2014). Transcription factor SOX9 plays a key role in the regulation of visual cycle gene expression in the retinal pigment epithelium. *J. Biol. Chem.* *289*, 12908–12921.
- McDonald, O.G., Wu, H., Timp, W., Doi, A., and Feinberg, A.P. (2011). Genome-scale epigenetic reprogramming during epithelial-to-mesenchymal transition. *Nat. Struct. Mol. Biol.* *18*, 867–874.
- Na, D., Son, H., and Gsponer, J. (2014). Categorizer: a tool to categorize genes into user-defined biological groups based on semantic similarity. *BMC Genomics* *15*, 1091.
- Nagasaki, H., Shinagawa, K., and Mochizuki, M. (1998). Risk factors for proliferative vitreoretinopathy. *Prog. Retin. Eye Res.* *17*, 77–98.
- Nazarieh, M., Wiese, A., Will, T., Hamed, M., and Helms, V. (2016). Identification of key player genes in gene regulatory networks. *BMC Syst. Biol.* *10*, 88.
- Pastor, J.C., de la Rua, E.R., and Martin, F. (2002). Proliferative vitreoretinopathy: risk factors and pathobiology. *Prog. Retin. Eye Res.* *21*, 127–144.
- Pratt, C.H., Vadigepalli, R., Chakravarthula, P., Gonye, G.E., Philp, N.J., and Grunwald, G.B. (2008). Transcriptional regulatory network analysis during epithelial-mesenchymal transformation of retinal pigment epithelium. *Mol. Vis.* *14*, 1414–1428.
- Rada-Iglesias, A., Bajpai, R., Swigut, T., Brugmann, S.A., Flynn, R.A., and Wysocka, J. (2011). A unique chromatin signature uncovers early developmental enhancers in humans. *Nature* *470*, 279–283.
- Radeke, M.J., Radeke, C.M., Shih, Y.H., Hu, J., Bok, D., Johnson, L.V., and Coffey, P.J. (2015). Restoration of mesenchymal retinal pigmented epithelial cells by TGFbeta pathway inhibitors: implications for age-related macular degeneration. *Genome Med.* *7*, 58.
- Rojas, J., Fernandez, I., Pastor, J.C., Garcia-Gutierrez, M.T., Sanabria, M.R., Brion, M., Coco, R.M., Ruiz-Moreno, J.M., Garcia-Arumi, J., Elizalde, J., et al. (2010). A strong genetic association between the tumor necrosis factor locus and proliferative vitreoretinopathy: the retina 4 project. *Ophthalmology* *117*, 2417–2423.e1-2.
- Roybal, C.N., Velez, G., Toral, M.A., Tsang, S.H., Bassuk, A.G., and Mahajan, V.B. (2018). Personalized proteomics in proliferative vitreoretinopathy implicate hematopoietic cell recruitment and mTOR as a therapeutic target. *Am. J. Ophthalmol.* *186*, 152–163.



- Saini, J.S., Corneo, B., Miller, J.D., Kiehl, T.R., Wang, Q., Boles, N.C., Blenkinsop, T.A., Stern, J.H., and Temple, S. (2017). Nicotinamide ameliorates disease phenotypes in a human iPSC model of age-related macular degeneration. *Cell Stem Cell* *20*, 635–647.e7.
- Salero, E., Blenkinsop, T.A., Corneo, B., Harris, A., Rabin, D., Stern, J.H., and Temple, S. (2012). Adult human RPE can be activated into a multipotent stem cell that produces mesenchymal derivatives. *Cell Stem Cell* *10*, 88–95.
- Sanabria Ruiz-Colmenares, M.R., Pastor Jimeno, J.C., Garrote Adrados, J.A., Telleria Orriols, J.J., and Yugueros Fernandez, M.I. (2006). Cytokine gene polymorphisms in retinal detachment patients with and without proliferative vitreoretinopathy: a preliminary study. *Acta Ophthalmol. Scand.* *84*, 309–313.
- Schiff, L., Boles, N.C., Fernandes, M., Nachmani, B., Gentile, R., and Blenkinsop, T.A. (2019). P38 inhibition reverses TGFbeta1 and TNFalpha-induced contraction in a model of proliferative vitreoretinopathy. *Commun. Biol.* *2*, 162.
- Skrypek, N., Goossens, S., De Smedt, E., Vandamme, N., and Berx, G. (2017). Epithelial-to-mesenchymal transition: epigenetic reprogramming driving cellular plasticity. *Trends Genet.* *33*, 943–959.
- Snead, D.R., James, S., and Snead, M.P. (2008). Pathological changes in the vitreoretinal junction 1: epiretinal membrane formation. *Eye (Lond.)* *22*, 1310–1317.
- Strunnikova, N.V., Maminishkis, A., Barb, J.J., Wang, F., Zhi, C., Sergeev, Y., Chen, W., Edwards, A.O., Stambolian, D., Abecasis, G., et al. (2010). Transcriptome analysis and molecular signature of human retinal pigment epithelium. *Hum. Mol. Genet.* *19*, 2468–2486.
- Takahashi, E., Nagano, O., Ishimoto, T., Yae, T., Suzuki, Y., Shinoda, T., Nakamura, S., Niwa, S., Ikeda, S., Koga, H., et al. (2010). Tumor necrosis factor-alpha regulates transforming growth factor-beta-dependent epithelial-mesenchymal transition by promoting hyaluronan-CD44-moesin interaction. *J. Biol. Chem.* *285*, 4060–4073.
- Tamiya, S., and Kaplan, H.J. (2016). Role of epithelial-mesenchymal transition in proliferative vitreoretinopathy. *Exp. Eye Res.* *142*, 26–31.
- Tiwari, N., Tiwari, V.K., Waldmeier, L., Balwierz, P.J., Arnold, P., Pachkov, M., Meyer-Schaller, N., Schubeler, D., van Nimwegen, E., and Christofori, G. (2013). Sox4 is a master regulator of epithelial-mesenchymal transition by controlling Ezh2 expression and epigenetic reprogramming. *Cancer Cell* *23*, 768–783.
- Zhang, Y., Zhao, D., Yang, S., Yao, H., Li, M., Zhao, C., Zhang, J., Xu, G.T., Li, H., and Wang, F. (2018). Protective effects of fucoidan on epithelial-mesenchymal transition of retinal pigment epithelial cells and progression of proliferative vitreoretinopathy. *Cell Physiol. Biochem.* *46*, 1704–1715.
- Zhao, M., Kong, L., Liu, Y., and Qu, H. (2015). dbEMT: an epithelial-mesenchymal transition associated gene resource. *Sci. Rep.* *5*, 11459.